BIOCHEMISTRY
including biophysical chemistry & molecular biology

Article

pubs.acs.org/biochemistry

Structural and Chemical Aspects of Resistance to the Antibiotic Fosfomycin Conferred by FosB from *Bacillus cereus*

Matthew K. Thompson,[†] Mary E. Keithly,[‡] Joel Harp,[§] Paul D. Cook,[∥] Kevin L. Jagessar,[†] Gary A. Sulikowski,[†,‡] and Richard N. Armstrong*[,†,‡,§]

[†]Department of Biochemistry, Vanderbilt University, Nashville, Tennessee 37232, United States
[‡]Department of Chemistry, Vanderbilt University, Nashville, Tennessee 37235, United States
[§]Center for Structural Biology, Vanderbilt University, Nashville, Tennessee 37235, United States
[∥]Department of Chemistry, Grand Valley State University, Allendale, Michigan 49401, United States

Supporting Information

ABSTRACT: The fosfomycin resistance enzymes, FosB, from Gram-positive organisms, are M^{2+}-dependent thiol tranferases that catalyze nucleophilic addition of either L-cysteine (L-Cys) or bacillithiol (BSH) to the antibiotic, resulting in a modified compound with no bacteriacidal properties. Here we report the structural and functional characterization of FosB from *Bacillus cereus* ($FosB^{Bc}$). The overall structure of $FosB^{Bc}$, at 1.27 Å resolution, reveals that the enzyme belongs to the vicinal oxygen chelate (VOC) superfamily. Crystal structures of $FosB^{Bc}$ cocrystallized with fosfomycin and a variety of divalent metals, including Ni^{2+}, Mn^{2+}, Co^{2+}, and Zn^{2+}, indicate that the antibiotic coordinates to the active site metal center in an orientation similar to that found in the structurally homologous manganese-dependent fosfomycin resistance enzyme, FosA. Surface analysis of the $FosB^{Bc}$ structures show a well-defined binding pocket and an access channel to C1 of fosfomycin, the carbon to which nucleophilic addition of the thiol occurs. The pocket and access channel are appropriate in size and shape to accommodate L-Cys or BSH. Further investigation of the structures revealed that the fosfomycin molecule, anchored by the metal, is surrounded by a cage of amino acids that hold the antibiotic in an orientation such that C1 is centered at the end of the solvent channel, positioning the compound for direct nucleophilic attack by the thiol substrate. In addition, the structures of $FosB^{Bc}$ in complex with the L-Cys-fosfomycin product (1.55 Å resolution) and in complex with the bacillithiol-fosfomycin product (1.77 Å resolution) coordinated to a Mn^{2+} metal in the active site have been determined. The L-Cys moiety of either product is located in the solvent channel, where the thiol has added to the backside of fosfomycin C1 located at the end of the channel. Concomitant kinetic analyses of $FosB^{Bc}$ indicated that the enzyme has a preference for BSH over L-Cys when activated by Mn^{2+} and is inhibited by Zn^{2+}. The fact that Zn^{2+} is an inhibitor of $FosB^{Bc}$ was used to obtain a ternary complex structure of the enzyme with both fosfomycin and L-Cys bound.

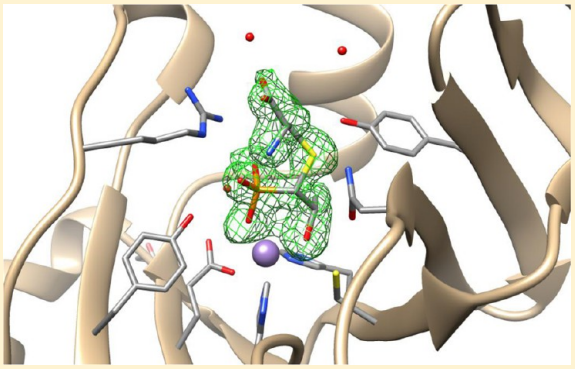

Microbial resistance to antibiotic compounds was recognized almost immediately after their introduction in the 1940s. The growing threat has culminated in the emergence of multiple-drug-resistant organisms that are invulnerable to treatment with several antimicrobial agents. Although the exact mechanism of antibiotic resistance can vary, antibiotic-modifying enzymes represent the most common mode of microbial survival and are, therefore, obvious targets for the development of new therapeutic agents. Combination therapies of administering antibiotics with additional enzyme inhibitors have already proven successful with the use of β-lactamase inhibitors to combat β-lactam resistant bacterial strains.

Fosfomycin, or (1*R*,2*S*)-epoxypropylphosphonic acid, is a safe, broad-spectrum antibiotic produced by various bacteria of the genus *Streptomyces*. It was initially characterized in 1969[1] and is used in the United States under the trade name Monurol. It is effective against both Gram-positive and Gram-negative bacteria owing to its ability to inhibit cell wall biosynthesis by inactivating the enzyme, UDP-*N*-acetylglucosamine-3-enolpyruvyltransferase or MurA. MurA catalyzes the initial step of peptidoglycan biosynthesis by transferring the enolpyruvyl moiety of phosphoenolpyruvate to the 3′-hydroxyl group of UDP-*N*-acetylglucosamine. The lactoyl moiety of the resulting UDP-*N*-acetylmuramic acid eventually provides a linker that bridges the glycan and peptide portions of peptidoglycan, a historically important target for antimicrobial agents. Fosfomycin is a phosphoenolpyruvate analog that covalently attaches to

Received: July 18, 2013
Revised: September 4, 2013
Published: September 5, 2013

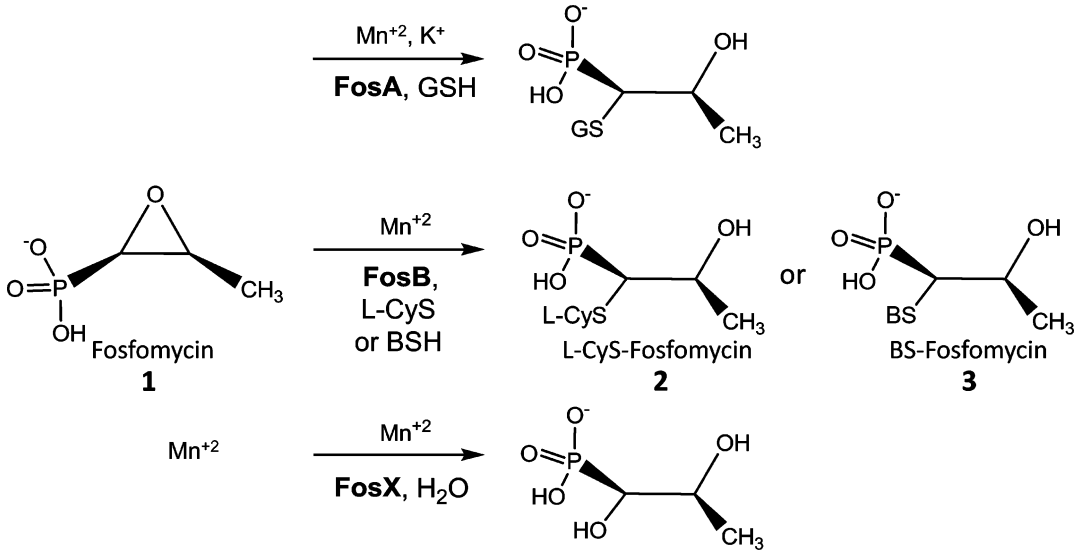

Figure 1. Reactions catalyzed by the fosfomycin resistance proteins FosA, FosB, and FosX. FosA is a Mn^{2+}- and K^{+}-dependent GSH transferase. FosB is a Mn^{2+}-dependent L-Cys or bacillithiol (BSH) transferase. FosX is a Mn^{2+}-dependent hydrolase. All three enzymes catalyze nucleophilic addition to the C1 of fosfomycin, subsequently opening the epoxide ring and destroying the efficacy of the drug.

an active site cysteine of MurA, irreversibly inhibiting the enzyme and shutting down peptidoglycan biosynthesis.[2−4]

Fosfomycin is most often prescribed for the treatment of urinary tract and gastrointestinal infections.[5,6] It has few human side effects and is eliminated from the body in its unmetabolized, active form. Therefore, it can be administered in a single 3 g dose that potentially circumvents two microbial resistance mechanisms, specifically, decreased cell permeability and active efflux pumping.[7] A significant disadvantage to its effectiveness, however, has been the emergence of enzymes that modify the antibiotic.

There are currently three distinct classes of fosfomycin resistance enzymes (Figure 1). FosA enzymes are Mn^{2+}- and K^{+}-dependent glutathione-S-transferases that catalyze nucleophilic addition of glutathione (GSH) to C1 of fosfomycin, opening the epoxide ring of the antibiotic and resulting in a modified compound with no bactericidal properties.[8−11] Genes encoding FosA have been identified in several Gram-negative bacterial species including the opportunistic human pathogen *Pseudomonas aeruginosa*.[12] FosX enzymes are Mn^{2+}-dependent hydrolases that catalyze the hydration of fosfomycin at C1 forming a vicinal diol and inactivating the antibiotic.[13,14] FosB enzymes were discovered in Gram-positive organisms such as *Staphylococcus aureus* and *Bacillis subtilis*[15,16] and catalyze the M^{2+}-dependent addition of L-cysteine (L-Cys) or bacillithiol (BSH) to C1 of fosfomycin.[17] The L-Cys transferase activity of FosB from *B. subtilis* is poor (k_{cat}/K_M^{thiol} ~180 M^{-1} s^{-1})[15] when compared to the GSH transferase activity of FosA from *P. aeruginosa* (k_{cat}/K_M^{thiol} ~1.7 × 10^5 M^{-1} s^{-1})[15] and is not sufficient to confer robust resistance to fosfomycin. However, recent kinetic analyses of the FosB enzymes from multiple organisms, conducted in the Armstrong laboratory, have indicated that bacillithiol is the preferred thiol substrate of the FosB enzymes in vitro.[17]

GSH is not produced by Gram-positive bacteria, which explains why the FosB enzymes have not evolved to be glutathione transferases. Instead, BSH is a abundant low molecular weight thiol found in nearly equal concentrations as L-Cys. BSH (Figure 2) was first isolated and identified in 2009 from *S. aureus* and *Deinococcus radiodurans*.[18] Similar to the

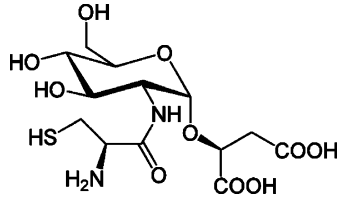

Figure 2. Structure of bacillithiol.

function of mycothiol in *Mycobacterium*, BSH serves as a substitute for glutathione in Gram-positive bacteria like *S. aureus*,[19,20] and BSH knockout/null cells exhibit a significant increase in their sensitivity to fosfomycin.[20] FosB catalyzes the addition of the cysteinyl-moiety of BSH to C1 of fosfomycin similar to FosA addition of GSH. These results have led to the FosB enzymes being classified as bacillithiol-S-transferases. The recent discovery of BSH, along with preliminary activity data, has motivated an effort to characterize the role of BSH in antimicrobial resistance of Gram-positive organisms.

Herein we report the kinetic analysis of FosB from *Bacillus cereus* ($FosB^{Bc}$) for the addition of either L-Cys or BSH to fosfomycin in the presence of Mg^{2+}, Ni^{2+}, Zn^{2+}, and Mn^{2+} and demonstrate that $FosB^{Bc}$ is a Mn^{2+}-dependent thiol transferase, like the homologous FosA and FosX enzymes, rather than the Mg^{2+}-dependent thiol transferase originally reported.[15] In addition, we demonstrate that, when activated by Mn^{2+}, $FosB^{Bc}$ has a preference for BSH over L-Cys as the cosubstrate for the inactivation of fosfomycin, confirming that $FosB^{Bc}$ is a bacillithiol-S-transferase. Furthermore, we show that $FosB^{Bc}$ is inhibited by Zn^{2+} for either L-Cys or BSH transferase activity. We also report nine 3D structures of $FosB^{Bc}$. In addition to the overall structure, we have cocrystallized the enzyme with fosfomycin and several divalent metals, including Ni^{2+}, Mn^{2+}, Co^{2+}, and Zn^{2+}, tested for activation in the kinetic analyses. Moreover, we have cocrystallized the enzyme with Mn^{2+}, L-Cys, and fosfomycin as well as Mn^{2+}, BSH, and fosfomycin, to obtain either the L-Cys-fosfomycin product [(1*R*,2*S*)-1-(*S*-L-cysteinyl)-2-hydroxypropylphosphonate] or the BS-fosfomycin [(1*R*,2*S*)-1-(*S*-bacillithiolyl)-2-hydroxypropylphosphonate] product in

dx.doi.org/10.1021/bi4009648 | *Biochemistry* 2013, 52, 7350−7362

the active site. The product structures show that the epoxide ring of fosfomycin has been opened because of nucleophilic addition of the thiol to C1 of the antibiotic. This renders the antibiotic inactive as it is no longer capable of serving as a suitable electrophilic substrate for inactivation of MurA. Finally, a ternary complex of $FosB^{Bc}$ cocrystallized with Zn^{2+}, L-Cys, and fosfomycin has been obtained that provides additional insight into the position of the nucleophile in the reaction.

MATERIALS AND METHODS

General Materials. Buffer salts were purchased from Research Products International Corporation. All crystallization materials were from Hampton Research. Metals were obtained as their chloride salts from J.T. Baker. L-Cysteine was purchased from Sigma Life Sciences. Fosfomycin disodium salt was from MP Biomedicals, LLC. BSH was synthesized as bacillithiol disulfide (BSSB) by the Vanderbilt Chemical Synthesis Core and reduced to BSH prior to use according to published procedures.[17]

Continuous ^{31}P NMR Activity Assays with Zn^{2+} and Mg^{2+}. Intein-tagged $FosB^{Bc}$ was expressed and purified for activity assays as previously described by our lab.[17] $FosB^{Bc}$ (0.5 μM) was equilibrated for 5 min with either 10 mM $MgCl_2$ or 100 μM $ZnCl_2$ and 8 mM fosfomycin in 20 mM HEPES (pH 7.0). The reaction was initiated by the addition of 4 mM BSH or L-Cys, transferred to an NMR tube, and allowed to react at 298 K. At various time points, a ^{31}P with ^{1}H decoupling NMR spectrum was collected using Bruker AV-400 MHz NMR. Analysis of the data was completed according to the method previously described.[17]

Continuous ^{31}P NMR Activity Assays with Ni^{2+}, Mn^{2+}, and Mg^{2}. Intein-tagged $FosB^{Bc}$ was expressed and purified for activity assays as previously described by our lab.[17] $FosB^{Bc}$ (0.25 μM) was equilibrated for 5 min with either 1 mM $MgCl_2$, 10 μM $NiCl_2$, or 10 μM $MnCl_2$ and 4 mM fosfomycin in 20 mM HEPES (pH 7.0). The reaction was initiated by the addition of 2 mM BSH or L-Cys, transferred to an NMR tube, and allowed to react at 298 K. At various time points, a ^{31}P with ^{1}H decoupling NMR spectrum was collected using Bruker DRX-500 MHz NMR. Analysis of the data was completed according to the method previously described by our lab.[17]

Protein Expression and Purification for Crystallography. A pET-20b expression plasmid containing the gene encoding nontagged WT FosB from *B. cereus* was transformed into *Escherichia coli* BL21 (DE3) cells. See ref 17 for plasmid preparation. The cells were plated on LB agar containing 100 ug/mL of ampicillin and incubated at 37 °C for approximately 16 h. Single colonies were isolated from the LB-agar plates and used to inoculate 2 mL of LB (Gibco) starter cultures (3 cultures for a total of 6 mL) containing 80 ug/mL of ampicillin. After approximately 8 h of incubation at 37 °C with shaking, 1 mL of starter growth was used to inoculate 1 L of Terrific Broth containing 80 ug/mL of ampicillin (6 L total). The 1 L cultures were grown at 37 °C with shaking for approximately 12 h (or until the OD_{600} reached ~1) and then induced with 0.5 mM IPTG. Upon induction with IPTG, the temperature was reduced to 25 °C, and the cells were allowed to grow for an additional 4 to 5 h. The cells were harvested by centrifugation at 5000*g* for 15 min.

The *E. coli* cell pellet was resuspended in 2 mL of lysis buffer (20 mM Tris HCL, pH 7.5) per gram of cell pellet. Lysozyme was added to the slurry at 1 mg/mL, and the mixture was stirred at 4 °C for 1 h. After 1 h of stirring, 5 mg of DNase and RNase were added, and the slurry was stirred at 4 °C for another hour. The slurry was sonicated to ensure complete lysing of cells, and the lysate was cleared by centrifugation at 35 000*g* for 30 min.

An ammonium sulfate precipitation was performed on the cleared lysate solution prior to any column purification. Fractions were precipitated at 5, 20, 40, 60, 80, and 95% ammonium sulfate. The fractions were analyzed by SDS-PAGE, and fractions containing the highest ratio of FosB to other proteins were combined for further purification. The protein was dialyzed overnight in 20 mM HEPES buffer (pH 7.0) to remove any residual lysis buffer or salt that could interfere with ion-exchange chromatography.

The collected fractions were pooled, concentrated, and loaded onto a GE Healthcare HiPrep DEAE FF 16/10 column, equilibrated with 20 mM HEPES (pH 7.0) using an Amersham Pharmacia Biotech ÄKTA*design* FPLC (equipped with a 50 mL super loop). With an estimated pI of 5.22, $FosB^{Bc}$ adheres to the DEAE material, and a purple hue can be seen on the column. The protein was eluted from the column at 2 mL/min using a gradient of 0−30% NaCl in the same buffer. Fractions were analyzed for purity by SDS-PAGE. The most pure fractions were collected, combined, and dialyzed overnight into 10 mM sodium phosphate (pH 7.0).

The protein, in 10 mM sodium phosphate buffer (pH 7.0), was subsequently loaded onto a 2.5 × 15 cm hydroxyapatite column (BioRad, Hercules, CA). $FosB^{Bc}$ adheres to the hydroxyapatite material. The protein was eluted from the column with an increasing concentration of phosphate. The protein eluted between 100 and 400 mM phosphate according to fractions analyzed by SDS-PAGE.

Finally, the protein was dialyzed into 50 mM sodium phosphate buffer (pH 7.5) containing 150 mM NaCl and 5 mM DTT. The protein was concentrated to approximately 1 mL with an Amicon 10K molecular weight cutoff membrane and loaded onto a GE Healthcare 26/60 Sephacryl column at 1 mL/min using an Amersham Pharmacia Biotech FPLC. Fractions were collected from the column at 0.5 mL each and analyzed for purity by SDS-PAGE

The purified $FosB^{Bc}$ protein was prepared with Mn^{2+}, Ni^{2+}, and Co^{2+} by dialyzing into 50 mM Bis-Tris (pH 6.0) with 5 mM EDTA and 2 mM 1,10-phenanthroline against 3 g Chelex resin. This ensured the removal of all metals. The protein was divided into fractions and dialyzed into 20 mM HEPES (pH 7.5) containing 200 μM of the respective divalent metal.

Protein Crystallization. Initial crystals of $FosB^{Bc}$ were grown using the hanging-drop vapor-diffusion method at 298 K by mixing 3 μL of protein solution (13 mg/mL in 20 mM HEPES buffer, pH 7.5) and 3 uL of reservoir solution (Hampton Research Index 92, 0.1 M magnesium formate and 15% PEG 3350 (w/v)) in a Hampton Research VDX plate. Crystallization hits were obtained in several different conditions, but those grown in HR Index 92 yielded the best diffraction. The final optimized conditions for each crystal are as follows. For $FosB^{Bc}$ with Zn^{2+} and sulfate and $FosB^{Bc}$ with Zn^{2+} and fosfomycin, crystals used for SAD phasing were obtained after mixing equal volumes (3 uL) of the protein solution (13 mg/mL in 20 mM HEPES buffer, pH 7.5) and reservoir solution (0.1 M magnesium formate and 12% (w/v) poly(ethylene glycol) 3350). The $FosB^{Bc}$ with Zn^{2+} and sulfate crystal used for molecular replacement was obtained after mixing equal volumes (3 uL) of the protein solution (13 mg/mL in 20 mM HEPES buffer (pH 7.5), 3 mM BSH, and 5 mM

dx.doi.org/10.1021/bi4009648 | *Biochemistry* 2013, 52, 7350−7362

Table 1. Data Collection and Refinement Statistics for FosB^{Bc}

	FosB·Zn·Sulf SAD	FosB·Zn·Sulf MR	FosB·Zn·Fos SAD	FosB·Ni·Fos SAD	FosB·Co·Fos SAD	FosB·Mn·Fos MR	FosB·Mn·Cys−Fos MR	FosB·Zn·Cys−Fos MR	FosBMn·BSH·Fos MR
PDB code	4JH1	4JH2	4JH3	4JH4	4JH5	4JH6	4JH7	4JH8	4JH9
space group	$P2_12_12_1$	$P2_12_12_1$	$P2_12_12_1$	$P2_12_12_1$	$P2_12_12_1$	$P2_12_12_1$	$P2_12_12_1$	$P2_12_12_1$	$P2_12_12_1$
unit-cell parameters									
a (Å)	64.45	64.34	64.34	64.41	64.33	64.49	64.29	64.31	56.48
b (Å)	68.20	68.09	68.27	68.54	68.23	68.69	68.31	68.54	64.48
c (Å)	69.60	69.77	69.90	70.44	69.88	70.09	70.18	69.85	83.91
data collection									
temperature (K)	100	100	100	100	100	100	100	100	100
wavelength (Å)	1.2823	1.0781	1.2823	1.4847	1.6046	1.1272	1.0781	1.0781	1.1272
resolution (Å)[a]	48.71−1.55 (1.61−1.55)	48.73−1.27 (1.29−1.27)	48.84−1.50 (1.55−1.50)	49.12−1.89 (1.93−1.89)	48.82−1.77 (1.80−1.77)	49.06−1.32 (1.34−1.32)	48.95−1.55 (1.58−1.55)	48.92−1.41 (1.43−1.41)	51.13−1.77 (1.83−1.77)
unique reflections	44 556	81 296	49 820	25 035	30 425	72 030	44 593	59 747	30 311
completeness (%)[a]	98.3 (85.2)	99.8 (99.2)	98.8(94.2)	98.4 (97.0)	98.8 (95.6)	97.8(99.9)	97.9(95.6)	99.1 (97.6)	99.2 (92.7)
R_{merge} (%)[b]	9.3 (52.9)	7.6(36.1)	9.5 (60.3)	12.6 (79.2)	9.5 (39.8)	5.1 (54.8)	6.6 (45.3)	4.8 (56.2)	8.4(60.1)
I/σ	27.5 (2.8)	46.0 (5.8)	23 (3.3)	36.6 (5.4)	64.2 (9.0)	32.19(2.0)	30.1 (3.6)	43.5 (3.0)	12.0(2.1)
redundancy	8.5 (4.7)	7.1 (7.0)	9.3 (7.1)	14.2(14.1)	13.3 (13.0)	4.0 (3.7)	7.4 (7.3)	7.3 (7.1)	4.7 (4.4)
refinement									
R_{work}/R_{free} (%)[c]	13.33/18.78	12.41/15.16	12.36/16.83	17.22/21.62	16.94/20.93	13.79/17.05	13.33/18.64	13.72/17.41	18.30/23.55
figure of merit (%)	90.25	93.69	91.79	87.48	87.94	91.01	91.13	92.02	82.16
average B factor (Å^2)									
all atoms	18.17	14.80	17.67	19.28	17.33	20.38	15.67	19.74	26.37
protein	17.01	13.34	16.25	19.03	16.90	19.62	14.55	18.66	26.15
water	28.59	24.20	28.25	23.53	22.77	26.82	23.11	26.83	28.67
no. of atoms									
protein	2640	2938	2707	2484	2546	2702	2682	2751	2524
water	258	379	315	142	185	250	259	253	135
rmsd from ideal									
bond length (Å)	0.021	0.023	0.021	0.020	0.023	0.023	0.021	0.023	0.019
bond angle (degrees)	1.96	2.28	1.95	2.02	2.20	2.20	2.07	2.30	1.97
Ramachandran plot (%)[d]									
most favored	234	234	234	235	234	234	232	232	230
allowed	16	16	16	15	16	16	18	18	20
disallowed	2	2	2	2	2	2	2	2	2

[a]Values in parentheses are for the highest resolution shell. [b]Rmerge = $\Sigma(|I - \bar{I}|)/\Sigma I \times 100$. [c]Rwork = $\Sigma|Fo - Fcl/\Sigma Fo \times 100$, where Fo is the observed structure factor amplitude and Fc is the calculated structure factor amplitude. [d]Values are given as the number of residues.

dx.doi.org/10.1021/bi4009648 | *Biochemistry* 2013, 52, 7350−7362

DTT) and reservoir solution (0.1 M magnesium formate and 9% (w/v) poly(ethylene glycol) 3350). For FosB^{Bc} with Ni^{2+}, Co^{2+}, or Mn^{2+} and fosfomycin, crystals were obtained after mixing equal volumes (3 uL) of the protein solution (13 mg/mL in 20 mM HEPES buffer (pH 7.5), 5 mM fosfomycin, and 200 μM M^{2+}) and reservoir solution (0.1 M magnesium formate and 12% (w/v) poly(ethylene glycol) 3350, 10% (w/v) poly(ethylene glycol) 3350, or 12% (w/v) poly(ethylene glycol) 3350 for Ni^{2+}, Co^{2+}, or Mn^{2+}, respectively). For FosB^{Bc} with Mn^{2+} and **2**, crystals were obtained after mixing equal volumes (3 uL) of the protein solution (13 mg/mL in 20 mM HEPES buffer (pH 7.5), 5 mM fosfomycin, 5 mM L-Cys, and 5 mM DTT; incubated for ~1 h on ice) and reservoir solution (0.1 M magnesium formate and 14% (w/v) poly(ethylene glycol) 3350). For FosB^{Bc} with Zn^{2+} and L-Cys/fosfomycin cosubstrates, crystals were obtained after mixing equal volumes (3 uL) of the protein solution (13 mg/mL in 20 mM HEPES buffer (pH 7.5), 5 mM fosfomycin, 5 mM L-Cys, and 5 mM DTT; incubated for ~1 h on ice) and reservoir solution (0.1 M magnesium formate and 8% (w/v) poly(ethylene glycol) 3350). For FosB^{Bc} with Mn^{2+} and **3**, crystals were obtained after mixing equal volumes (3 uL) of the protein solution (13 mg/mL in 20 mM HEPES buffer (pH 7.5), 8 mM fosfomycin, 8 mM BSH, and 5 mM DTT; incubated for ~1 h on ice) and reservoir solution (0.1 M magnesium formate and 14% (w/v) poly(ethylene glycol) 3350). All crystals were cryoprotected in the mother solution and 15% glycerol prior to freezing in liquid nitrogen and data collection.

Data Collection and Refinement. Screening for the diffraction of crystals was performed at the Biomolecular Crystallography Facility in the Vanderbilt University Center for Structural Biology using a Bruker-Nonius Microstar rotating anode X-ray generator equipped with a Proteum PT135 CCD area detector mounted on an X8 kappa goniometer with Montel confocal multilayer optics. Crystals were maintained at 100 K using a Bruker KryoFlex cryostat.

Diffraction data for all crystals were collected at 100 K on the LS-CAT 21-ID beamline at the APS synchrotron facility. The collected diffraction data sets were processed with HKL2000.[21] Phasing of diffraction data was done either by molecular replacement using PHASER[22] or by SAD phasing using SHELXD/E.[23] For SAD phasing, the presence of the anomalous scatterer was confirmed and the peak wavelength determined by X-ray fluorescence. Two anomalous scatterers were located in the asymmetric unit corresponding to two active sites in the enzyme. In the case of SAD phasing, initial models were constructed using ARPwARP.[24] For molecular replacement, the first model output and refined from ARPwARP was used as the initial search model. All crystals belong to the $P2_12_12_1$ space group and contain 276 amino acids in the asymmetric unit, which represents the complete FosB enzyme. Manual model building for each structure was performed using Coot model building software.[25] Water molecules were placed with the Coot routine, Find Waters. The final models were obtained by iterative cycles of model building in Coot and structure refinement using Refmac5[26] in the CCP4 suite of programs (Collaborative Computational Project, 1994). All protein figures were prepared with Chimera.[27] Data collection and refinement statistics are given in Table 1.

X-ray Fluorescence Spectroscopy. All X-ray fluorescence spectra of the crystals were collected at 100 K on the LS-CAT 21-ID beamline at the APS synchrotron facility and used without further processing.

RESULTS

Kinetic Analysis. The metal activation of FosB^{Bc} by Mg^{2+} and Ni^{2+} has been reported.[17] Nevertheless, divalent metal activation of the FosB enzymes remains unclear and may be different for different organisms possessing the enzyme. In this report, kinetic analyses for the addition of either L-Cys or BSH to fosfomycin in the presence of Mg^{2+}, Ni^{2+}, Zn^{2+}, and Mn^{2+} were conducted to probe further the appropriate divalent metal activation of FosB^{Bc} (Figure 3). Both fosfomycin and the thiol-

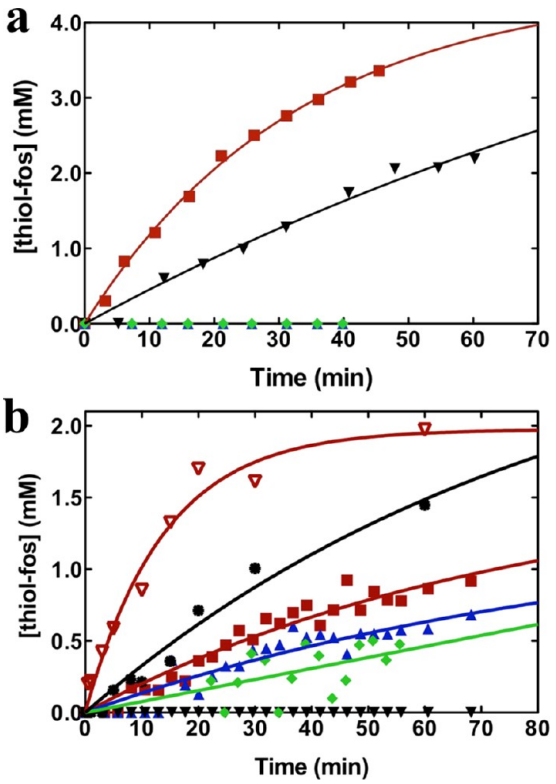

Figure 3. (a) Time-course kinetics for the FosB^{Bc}-catalyzed addition of BSH or L-Cys to fosfomycin in the presence of Mg^{2+} or Zn^{2+}. Reactions were carried out at 25 °C in 20 mM HEPES, pH 7.0, with 8 mM fosfomycin and 0.5 μM enzyme in the presence of 4 mM BSH and 10 mM Mg^{2+} (red square), 4 mM L-Cys and 10 mM Mg^{2+} (black triangle), 4 mM BSH and 100 μM Zn^{2+} (blue triangle), and 4 mM L-Cys and 100 μM Zn^{2+} (green diamond). (b) Time course of the FosB^{Bc}-catalyzed addition of BSH or L-Cys to fosfomycin in the presence of Mg^{2+}, Ni^{2+}, or Mn^{2+}. Reactions were carried out at 25 °C in 20 mM HEPES, pH 7.0, with 4 mM fosfomycin and 0.25 μM enzyme in the presence of 2 mM BSH and 10 μM Mn^{2+} (open red triangle), 2 mM BSH and 10 μM Ni^{2+} (red square), 2 mM BSH and 1 mM Mg^{2+} (blue triangle), 2 mM L-Cys and 10 μM Mn^{2+} (black circle), 2 mM L-Cys and 10 μM Ni^{2+} (black triangle), and 2 mM L-Cys and 1 mM Mg^{2+} (green diamond).

fosfomycin product can be readily detected by ^{31}P NMR. The initial reactions were conducted at 298 K in 20 mM HEPES (pH 7.0) with 8 mM fosfomycin and 0.5 μM FosB^{Bc} in the presence of 4 mM BSH and 10 mM Mg^{2+}, 4 mM L-Cys and 10 mM Mg^{2+}, 4 mM BSH and 100 μM Zn^{2+}, or 4 mM L-Cys and 100 μM Zn^{2+} (Figure 3a). The concentration of Mg^{2+} was originally selected to be much greater than K_{act} (~200 uM) for the homologous FosB enzyme from *B. subtilis*.[15] The results

dx.doi.org/10.1021/bi4009648 | *Biochemistry* 2013, 52, 7350−7362

quickly revealed that Zn^{2+} is a potent inhibitor of L-Cys or BSH activity. Additional reactions to test the activity of Mn^{2+} and Ni^{2+}, along with Mg^{2+}, were conducted at 298 K in 20 mM HEPES (pH 7.0) with half of the enzyme and cosubstrate concentrations (Figure 3b). This was necessary because the reaction is so efficient with Mn^{2+} and BSH that the initial observable time point via the ^{31}P NMR method using the higher concentrations was beyond completion. In addition, the concentration of Mg^{2+} was reduced to 1 mM to more adequately represent the prevailing intracellular concentration of the metal. Reduction of Mg^{2+} had no effect on the results. From the data, the apparent k_{cat} values for $FosB^{Bc}$ with each metal and thiol substrate were estimated. The apparent k_{cat} values for $FosB^{Bc}$ with BSH and Mn^{2+}, Ni^{2+}, or Mg^{2+} are 26.7, 1.3, and 1.0 s^{-1}, respectively, and the apparent k_{cat} values for $FosB^{Bc}$ with L-Cys and Mn^{2+}, Ni^{2+}, or Mg^{2+} are 2.0, 0.6 s^{-1}, and unable to be determined, respectively. The results demonstrate that $FosB^{Bc}$ has a preference for BSH over L-Cys, with metal activation in vitro as follows: $Mn^{2+} > Ni^{2+} > Mg^{2+}$. These results indicate that $FosB^{Bc}$ is a Mn^{2+}-dependent bacillithiol-S-transferase.

Crystal Structure Determination. *$FosB^{Bc}$ with Zinc and Sulfate (SAD Phasing).* (PDB 4JH1) The crystal structure of $FosB^{Bc}$·Zn^{2+} was refined to 1.55 Å resolution (Figure S1). The presence of a high concentration of zinc was confirmed by an X-ray fluorescence scan of the crystal prior to collection of diffraction data (Figure S2). Subsequently, the diffraction data were collected at a wavelength of 1.28 Å, the K_α absorption edge of Zn^{2+}, and Zn^{2+} was used to model the density.

$FosB^{Bc}$ with Zinc and Sulfate (Molecular Replacement). (PDB 4JH2) Cocrystallization of the enzymes in the presence of BSH resulted in significantly better quality crystals even though the BSH molecule was never observed in the structure. The data set resulted in a 1.27 Å resolution structure of $FosB^{Bc}$ with zinc and sulfate in the active site, solved by molecular replacement.

$FosB^{Bc}$ with Zinc and Fosfomycin (SAD Phasing). (PDB 4JH3) A high-resolution crystal structure of $FosB^{Bc}$·Zn^{2+} with fosfomycin bound to the metal ion in the active site was obtained to 1.49 Å resolution (Figures S1 and S3). Similar to the $FosB^{Bc}$·Zn^{2+}·sulfate structure (PDB 4JH1), the initial phases were determined using Zn^{2+} SAD phasing at 1.28 Å wavelength. The anomalous density map, contoured at 5σ, is displayed in Figure S3 and outlines the location of the modeled Zn^{2+} metal ions.

$FosB^{Bc}$ with Nickel and Fosfomycin (SAD Phasing). (PDB 4JH4) A high-resolution crystal structure of $FosB^{Bc}$ with Ni^{2+} and fosfomycin bound in the active site was obtained to 1.89 Å resolution (Figure S4). The initial phases were determined using Ni^{2+} SAD phasing at 1.48 Å wavelength, the K_α absorption edge of Ni^{2+}. An X-ray fluorescence scan of the crystal prior to diffraction data collection indicated the presence of Ni^{2+} (Figure S5). The anomalous density map, modeled using Ni^{2+}, is displayed in Figure S4 and marks the location of the Ni^{2+} metal ions.

$FosB^{Bc}$ with Cobalt and Fosfomycin (SAD Phasing). (PDB 4JH5) The crystal structure of $FosB^{Bc}$ with Co^{2+} and fosfomycin bound in the active site was refined to 1.77 Å resolution (Figure S6). The initial phases were determined using Co^{2+} SAD phasing at 1.61 Å wavelength. Again, an X-ray fluorescence scan of the crystal prior to diffraction data collection indicated the presence of Co^{2+} (Figure S7), and the diffraction data were collected at the K_α absorption edge of Co^{2+}, 1.61 Å. Thus, Co^{2+} was used to model the resulting density. The anomalous density map is displayed in Figure S6 around the modeled Co^{2+} metal ions.

$FosB^{Bc}$ with Manganese and Fosfomycin (Molecular Replacement). (PDB 4JH6) The crystal structure of $FosB^{Bc}$ with Mn^{2+} and fosfomycin bound in the active site was refined to 1.32 Å resolution (Figures 4 and 5a). The structure was solved by molecular replacement using the initial structure of $FosB^{Bc}$·Zn^{2+} where the Zn^{2+} was removed from the coordinate file before the phasing process. A SAD experimental data set was not collected for this crystal because of the 1.89 Å K_α absorption edge of Mn^{2+}. The longer wavelength can damage protein crystals during data collection. Nevertheless, an X-ray fluorescence scan of the crystal indicated the presence of Mn^{2+} (Figure S8), and because the protein was prepared with Mn^{2+} and crystallized in the same manner as that for Ni^{2+} and Co^{2+} that yielded excellent SAD phasing data, it is safe to assume that the metal-ion density is that of Mn^{2+}.

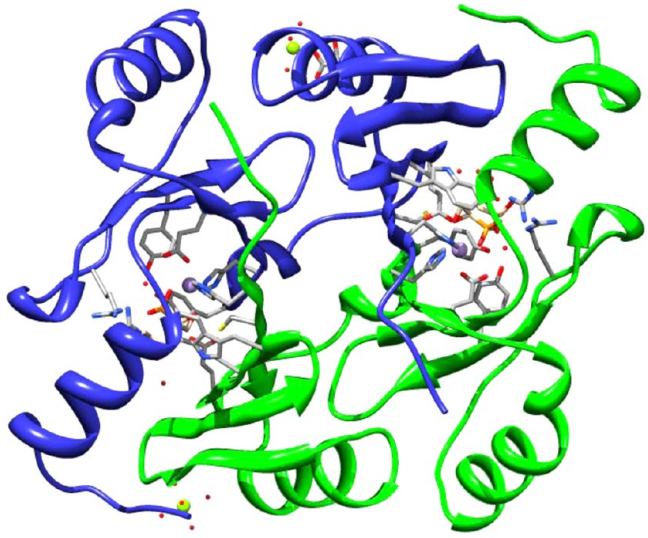

Figure 4. Overall X-ray crystal structure of the FosB protein from *Bacillus cereus* in complex with Mn^{2+} and fosfomycin at 1.32 Å resolution (PDB 4JH6). In the final refinement, R_{work} = 13.79% and R_{free} = 17.05%.

$FosB^{Bc}$ with Manganese and L-Cysteine-Fosfomycin Product (Molecular Replacement). (PDB 4JH7) The $FosB^{Bc}$·Mn^{2+}·**2** product complex was obtained to 1.55 Å resolution (Figure 5b). The structure was solved by molecular replacement. The presence of Mn^{2+} in the crystal was verified by X-ray fluorescence. The B factors for each of the metal sites in the crystal indicate Mn^{2+} ions are a good fit for the observed electron density, as the B factor for Mn^{2+} in one site is 8.1 $Å^2$, and the coordinating amino acids have average B factors of 7.9, 7.1, and 6.7 $Å^2$ for His7, His66, and Glu115, respectively. A library file in CIF format for (1*R*,2*S*)-1-(*S*-L-cysteinyl)-2-hydroxypropylphosphonate was created using the online PRODRG Server[28] and inserted into the model during the final refinement.

$FosB^{Bc}$ with Zinc, Fosfomycin, and L-Cysteine (Molecular Replacement). (PDB 4JH8) The crystals of $FosB^{Bc}$ grown in the presence of Zn^{2+}, fosfomycin, and L-Cys yielded electron density that is neither clearly the product nor clearly the fosfomycin and cysteine cosubstrates (Figure 5c). The structure was solved by molecular replacement. The density for the C1

dx.doi.org/10.1021/bi4009648 | *Biochemistry* 2013, 52, 7350−7362

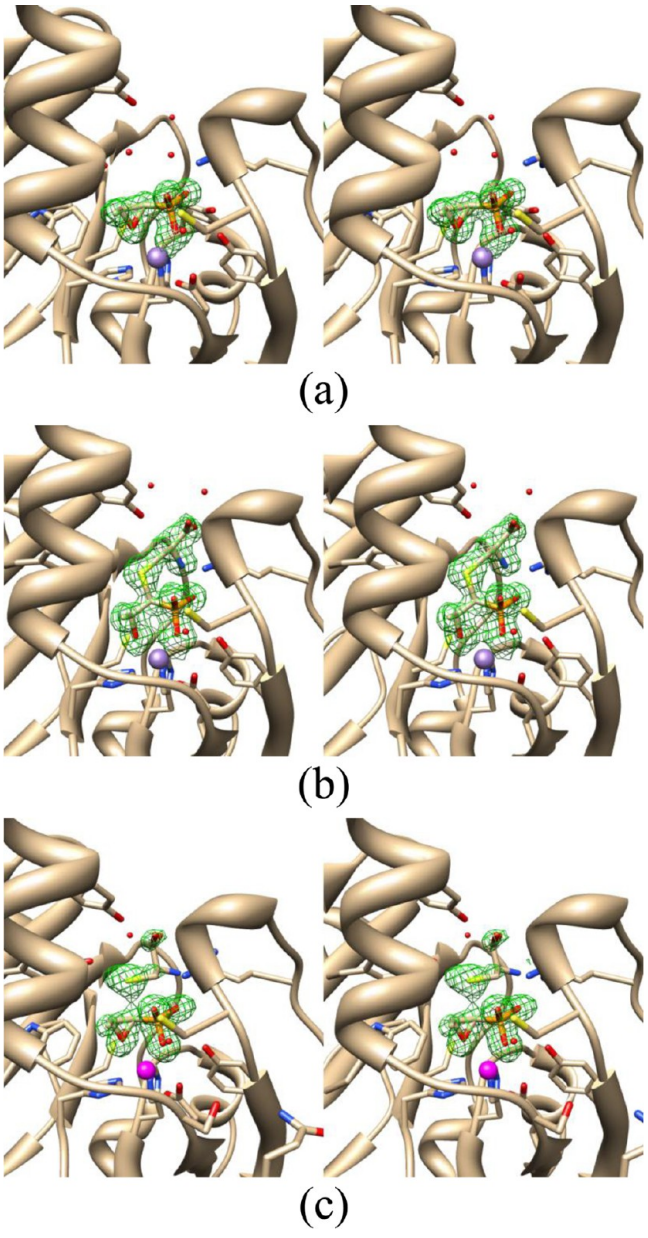

Figure 5. Stereo views of (a) FosB^{Bc}·Mn^{2+}·**1** (PDB 4JH6), (b) FosB^{Bc}·Mn^{2+}·**2** (PDB 4JH7), and (c) FosB^{Bc}·Zn^{2+}·**1**·L-Cys (PDB 4JH8). Difference densities are the $2F_o-F_c$ maps calculated before addition of the ligands to the coordinate files and are contoured at 3σ. The electron density in (panel a shows the position of **1** coordinated to Mn^{2+}. The electron density in panel b clearly shows **2** coordinated to Mn^{2+}, and the density for C1 of **1** is sp^3 hybridized following nucleophilic attack by the L-Cys thiol. The electron density in panel c shows **1** coordinated to Zn^{2+}, with the density for the C1 carbon of **1** more substrate-like in geometry than that of panel b, indicating no product formation. The strong electron density above C1 likely belongs to sulfur. The ambiguity in the rest of the density for the L-Cys is probably due to a combination of occupancy and multiple conformations in the crystal.

carbon of fosfomycin appears to be more substrate-like in character than that of the product complex (compare panel c to panel a of Figure 5). Moreover, there is strong electron density above C1 that is almost certainly that of sulfur. The ambiguity in the rest of the density for the cysteine likely arises from a combination of occupancy and multiple conformations in the solvent channel.

FosB^{Bc} with Mn^{2+} and Bacillithiol-Fosfomycin Product Complex (Molecular Replacement). (PDB 4JH9) The FosB^{Bc}·Mn^{2+}·**3** product complex was obtained to 1.55 Å resolution. The structure was solved by molecular replacement. The same (1*R*,2*S*)-1-(*S*-L-cysteinyl)-2-hydroxypropylphosphonate product was used to model the observed density in the active site because the glucosamine-malate domain of BSH was not observed (Figure S9).

Structural Characterization of FosB^{Bc}. As anticipated, the overall structure of FosB^{Bc} (Figures 4, S3, S4, and S6) reveals that the enzyme is a homodimer and belongs to the vicinal oxygen chelate (VOC) superfamily of enzymes similar to FosA, FosX,[12,13,29] and the recently deposited FosB structure from *Bacillus anthracis* (FosB^{Ba}, PDB 4IR0). The VOC superfamily of metalloenzymes is characterized by a 3D domain-swapped arrangement of tandem $\beta\alpha\beta\beta\beta$ motifs in which both subunits of the homodimer participate in coordination of each metal ion and formation of the U-shaped active sites in the enzyme.[30] All of the reported structures maintain the overall arrangement with little variation. The overall rmsd for all atoms of the nine reported FosB^{Bc} structures is 0.32 Å, calculated with Chimera.[27]

Like the FosA and FosX enzymes, two histidines and a glutamic acid in FosB^{Bc} serve as the protein ligands that coordinate the metal ion. Specifically for FosB^{Bc}, they are His7, His66, and Glu115. In the FosB^{Bc}·Zn^{2+}·sulfate structure (PDB 4JH2), the Zn^{2+} adopts a tetrahedral coordination geometry, with a sulfate oxygen occupying the fourth coordinate site of the inner-coordination sphere of the metal. The $2F_o-F_c$ difference density calculated prior to the addition of sulfate to the coordinate file clearly establishes the presence of the sulfate ion coordinated to Zn^{2+} (Figure S1). The ligand–metal distances are 2.02, 1.99, and 2.01 Å for His7, His66, and Glu115, respectively, with a metal–sulfate oxygen distance of 1.90 Å.

Structure of FosB^{Bc} with M^{2+} and Fosfomycin. Coordination of fosfomycin by the various divalent metals tested is similar in each structure. The $2F_o-F_c$ difference map, calculated before addition of fosfomycin to the coordinate files, clearly establishes the presence of the antibiotic coordinated to Zn^{2+} Ni^{2+}, Co^{2+}, or Mn^{2+} (PDBs 4JH1, 4JH4, 4JH5, and 4JH6; Figures 5a and S1). Similar to that observed for FosA with bound fosfomycin, the geometry of metal coordination for FosB^{Bc} with bound fosfomycin can be described as highly distorted, five-coordinate trigonal bipyramidal. His7, His66, and the phosphonate oxygen occupy the equatorial sites, whereas Glu115 and the oxirane oxygen of fosfomycin occupy the axial sites.

FosB^{Bc} with Mn^{2+} and L-Cysteine-Fosfomycin Product Complex and Stereochemical Configuration at C1 of the Product. The FosB^{Bc}·Mn^{2+}·**2** product complex (PDB 4JH7) was obtained in the presence of L-Cys, fosfomycin, and the FosB^{Bc}·Mn^{2+} enzyme. The $2F_o-F_c$ difference map outlines the product molecule in the active site of FosB^{Bc} (Figure 5b). In the structure, the epoxide ring of fosfomycin has been opened via nucleophilic addition of L-Cys to C1 of fosfomycin. The C1 of fosfomycin is sp^3 hybridized, and strong electron density is observed for the sulfur. The L-Cys-fosfomycin product molecule was constructed in PRODRG[28] according to the stereochemistry originally reported by Bernat et al, which was biosynthesized using the FosA enzyme.[31] Thus, the resulting **2**

dx.doi.org/10.1021/bi4009648 | *Biochemistry* 2013, 52, 7350–7362

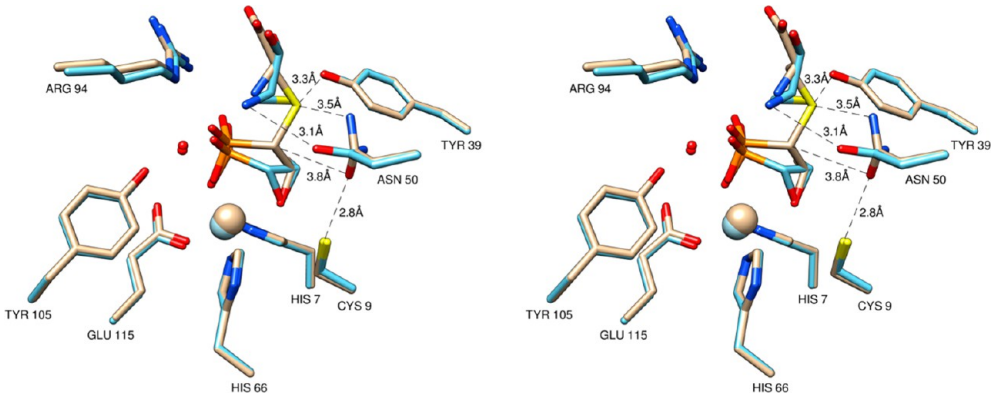

Figure 6. Stereo view for the superposition of the FosB^{Bc}·Mn^{2+}·**2** structure (PDB 4JH7) and the FosB^{Bc}·Zn^{2+}·**1**·L-Cys ternary structure (PDB 4JH8). Although the positions of all other amino acids stay the same, Asn50 in the ternary complex is rotated approximately 90° relative to the product complex. Rotation of Asn50 about the C_β−C_γ bond is the only significant difference observed in the reported structures of FosB^{Bc}. The conserved residues, Tyr39 and Asn50, likely work in a concerted manner to ionize and stabilize the approaching thiolate during nucleophilic attack of the antibiotic.

product can be correctly identified as (1*R*,2*S*)-1-(*S*-L-cysteinyl)-2-hydroxypropylphosphonate, the same product as that reported for FosA.[31] Inversion of configuration at C1 indicates that the reaction proceeds via direct S_N2 addition of the thiol to the oxirane carbon.

The ligand−metal distances in the FosB^{Bc}·Mn^{2+}·**2** structure are 2.16, 2.16, and 2.07 Å for His7, His66, and Glu115, respectively. The metal to phosphonate oxygen distance is 2.02 Å, with a metal to oxirane oxygen distance of 2.36 Å.

FosB^{Bc} with Zinc and Ternary Complex (Molecular Replacement). The crystals of FosB^{Bc} grown in the presence of Zn^{2+}, fosfomycin, and L-Cys yielded electron density that most closely resembles the fosfomycin and L-Cys cosubstrates (Figure 5c). The density for the C1 carbon of fosfomycin is more substrate-like in geometry than that of the product complex (Figure 5b). In addition, the strong electron density above C1 has a peak of 17.30σ, too intense for even the most well-ordered water molecules. Moreover, when refined with L-Cys, the sulfur atom has a B factor of 27.1 Å^2 averaged over the two sites. This value compares quite well with the overall B factor for the structure of 19.7 Å^2. Furthermore, the oxygen of Tyr39 is 3.25 Å from the sulfur, and the location of the sulfur superimposes that of the thioether of **2** in the FosB^{Bc}·Mn^{2+}·**2** structure. Finally, the distance between C1 of **1** and the sulfur is 2.79 Å. This distance is significantly shorter than the theoretical van der Waals interaction of 3.50 Å yet much longer than a typical carbon−sulfur single bond (1.83 Å) and likely represents the location of the sulfur when it is poised for nucleophilic attack of the antibiotic. The ambiguity in the rest of the density for the L-Cys probably arises from a combination of occupancy and multiple conformations throughout the crystal. Nevertheless, there is enough density to correctly establish the location of the L-Cys sulfur.

This structure is not intended to serve as evidence for the location of the L-Cys binding site. That location is made crystal clear by the FosB^{Bc}·Mn^{2+}·**2** structure described above. Rather, this structure is presented as a ternary structure with both substrates in the active site, which was an anticipated result given that Zn^{2+} is a potent inhibitor of enzymatic activity for FosB^{Bc} (Figure 3).

The most interesting aspect of this structure is the position of Asn50. The electron density for Asn50 in this structure has the residue oriented perpendicular to that of all of the other structures, an orientation that positions the O_δ of Asn50 4.13 Å from C1 of fosfomycin and N_δ of Asn50 4.20 Å from the sulfur of L-Cys. Superposition of the Zn^{2+} ternary-complex structure and the Mn^{2+} product-complex structure shows that, whereas the positions of all other amino acids stay the same, Chi2 of Asn50 in the ternary complex is rotated approximately 90° relative to the product complex (Figure 6). This structure of FosB^{Bc} is the only structure that shows significant displacement of any amino acid.

FosB^{Bc} with Mn^{2+} and BS-Fosfomycin Product Complex (Molecular Replacement). The FosB^{Bc}·Mn^{2+}·**3** product complex (PDB 4JH9) was obtained in the presence of BSH, fosfomycin, and the FosB^{Bc}·Mn^{2+} enzyme. The FosB^{Bc}·Mn^{2+}·**3** complex was determined via the same crystallization methods as those used to obtain the FosB^{Bc}·Mn^{2+}·**2** complex. FosB^{Bc} was prepared with Mn^{2+} and incubated with BSH and fosfomycin for approximately 1 h before the solution was used for crystallization trials.

In the structure, the epoxide ring of fosfomycin has been opened via nucleophilic addition of BSH. However, electron density for the complete **3** is not observed. Rather, the electron density more closely resembles that of **2** even though L-Cys was never introduced into the crystallization conditions. It is unclear if the L-Cys moiety has somehow been removed from the glucosamine-malate portion of BSH or if the glucosamine-malate moiety is simply not homogeneous in the crystal. Either scenario would give rise to the observed density that resembles **2** only. However, the second scenario is more plausible. First, Roberts et al. reported a purification procedure for **3** that involves heating for 10 min at 85 °C followed by derivatization with AQC (6-aminoquinolyl-*N*-hydroxysuccinimidyl carbamate) at pH 8.8 and then adjustment to pH 5.5 for HPLC analysis,[32] thereby establishing the inherent stability of **3** over a broad temperature and pH range. Second, Roberts et al. were unable to dock a BSH molecule into the crystal structure of FosB from *B. anthracis* (FosB^{Ba}, PDB 4IR0) and attributed the failure to a possible conformational change that may take place in the enzyme when BSH binds.[32] Protein flexibility is critical for proper enzymatic function, and the rigidity of the crystal may prevent proper seating of the BSH molecule to the enzyme. Finally, the unit cell dimensions for this crystal (PDB 4JH9) are different than the others reported. The average unit cell dimensions for the other eight structures are 64.37 ± 0.07,

dx.doi.org/10.1021/bi4009648 | *Biochemistry* 2013, 52, 7350−7362

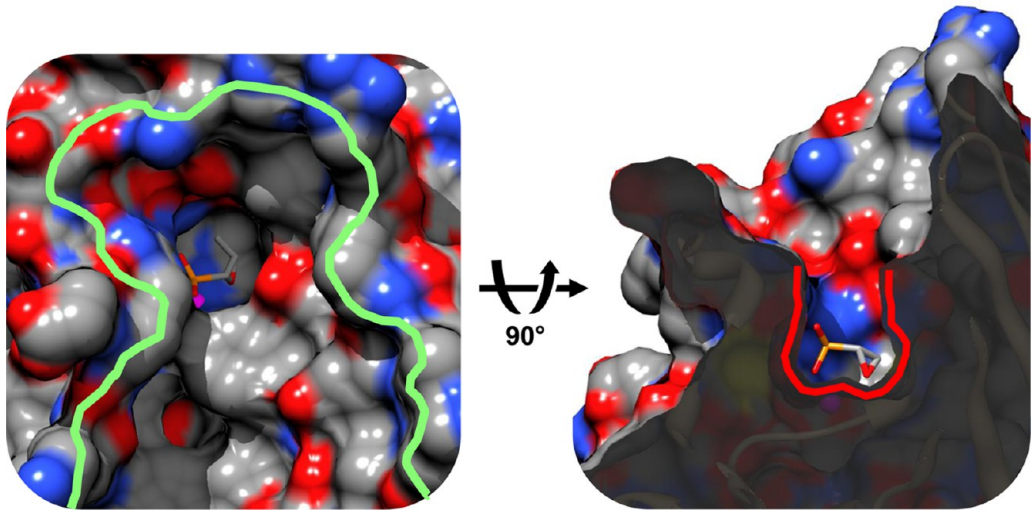

Figure 7. (left) Top-view of a channel from the surface of the protein into the active site (left). The green line contours a depression in the surface of the protein large enough to accommodate BSH. (right) Narrowing of the channel near fosfomycin (shown in stick representation). The narrow section (outlined in red) is large enough to accommodate either L-Cys or the cysteinyl moiety of BSH. Note that the backside of the oxirane carbon to be attacked is positioned in the middle of the solvent channel. This figure was made with PDB 4JH3.

68.36 ± 0.21, and 69.96 ± 0.26 Å, whereas the unit cell dimensions for the crystal with **3** are 56.48, 64.48, and 83.91 Å (Table 1), indicating a significant difference in crystal packing. Given the stability of **3** and the fact that L-Cys was never introduced into the crystallization conditions, it is reasonable to assume that **3** is present and simply not observed in the electron density. Thus, what is observed in the structure is the phosphonate end of the product molecule tethered to the Mn^{2+} metal within the enzyme, whereas the remainder of the molecule is solvent exposed and disordered on the surface of the enzyme within the crystal (Figure S9).

DISCUSSION

Our initial crystals of $FosB^{Bc}$ (PDBs 4JH1, 4JH2, and 4JH3) contained Zn^{2+} in the active site similar to the structure of FosB from *B. anthracis* (PDB 4IR0). The metal was confirmed via X-ray fluorescence and SAD phasing from the K_α edge of Zn^{2+}. These crystals were grown from preparations of $FosB^{Bc}$ purified from cells grown in terrific broth media without further manipulation to remove or add specific metals. Therefore, Zn^{2+} was the divalent metal "selected" by the enzyme from the growth conditions. Given that both our initial crystals and the crystal of $FosB^{Ba}$ had Zn^{2+} in the active, we tested the activation of $FosB^{Bc}$ for both L-Cys and BSH transferase activity using the enzyme prepared specifically with Zn^{2+}. The results indicate that Zn^{2+} inhibits both the L-Cys and BSH transferase activity of $FosB^{Bc}$ and is ultimately what prompted further kinetic analysis of the $FosB^{Bc}$ enzyme (Figure 3a).

Preliminary research into divalent metal activation of FosB established the activation order for FosB from *B. subtilis* as $Ni^{2+} \sim Mg^{2+} > Mn^{2+} > Fe^{2+} > Cu^{2+} > Ca^{2+} \sim Co^{2+} > Zn^{2+}$ with L-Cys as the thiol substrate.[15] Recent access to BSH has allowed the screening of several FosB enzymes for bacillithiol-S-tranferase activity. The new results demonstrate that at least four known FosB enzymes, from *Staphylococcus aureus* ($FosB^{Sa}$), *Bacillus subtilis* ($FosB^{Bs}$), *Bacillus anthracis* ($FosB^{Ba}$), and *Bacillus cereus* ($FosB^{Bc}$), have a preference for BSH as the thiol substrate.[17] The more extensive kinetic analysis of $FosB^{Bc}$ presented here demonstrates a preference for BSH over L-Cys and establishes the metal activation of $FosB^{Bc}$ in vitro to be $Mn^{2+} > Ni^{2+} > Mg^{2+} > Zn^{2+}$ (Figure 3a,b). This divalent metal activation of $FosB^{Bc}$ is in excellent agreement with the homologous classes of fosfomycin resistance enzymes, FosA and FosX, where both are most activated by Mn^{2+} and show only very minimal activity with Zn^{2+} in the presence of their respective nucleophiles.[10,13]

The preference of $FosB^{Bc}$ for BSH over L-Cys suggests that the glucosamine-malate domain of the BSH molecule is important for substrate recognition. Substitution of the malate motif of BSH with either an *O*-methyl or *O*-benzyl aglycone group results in a 10- and 18-fold increase in K_m, respectively, of the substrate for FosB from *S. aureus*.[32] Thus, the thermodynamic driving force of nucleophilic addition is likely interaction of the glucosamine-malate domain with the surface of the enzyme.

Surface analysis of the $FosB^{Bc}$ structures revealed a well-defined pocket and access channel to C1 of fosfomycin, the carbon to which nucleophilic addition of the thiol occurs. The pocket and access channel are appropriate in size and shape to accommodate L-Cys or BSH. Fosfomycin is positioned in the enzyme such that the backside of the oxirane carbon to be attacked is directly centered at the end of the solvent access channel (Figure 7).

The role of the binding pocket and access channel are made clear by either the $FosB^{Bc}{\cdot}Mn^{2+}{\cdot}$**2** product complex (PDB 4JH7) or the $FosB^{Bc}{\cdot}Mn^{2+}{\cdot}$**3** product complex (PDB 4JH9). In either structure, nucleophilic addition of the thiolate to C1 of **1** has occurred at the end of the channel (Figure 8, PDB 4JH7 shown). The opening of the binding pocket from the access channel begins at the C_α end of the cysteinyl moiety, where the remainder of the bacillithiol domain would be connected through the secondary amine of **3**. Unfortunately, in PDB 4JH9, the complete **3** was not observed seated in the binding pocket of the crystal for reasons described vide supra.

The fosfomycin molecule, coordinated to the metal, is surrounded by a cage of amino acids positioned appropriately to anchor the antibiotic in the aforementioned orientation (Figure 9). Inspection of the cage reveals it has both polar and nonpolar ends to accommodate fosfomycin. The polar phosphonate group of the antibiotic is coordinated to the

dx.doi.org/10.1021/bi4009648 | *Biochemistry* 2013, 52, 7350−7362

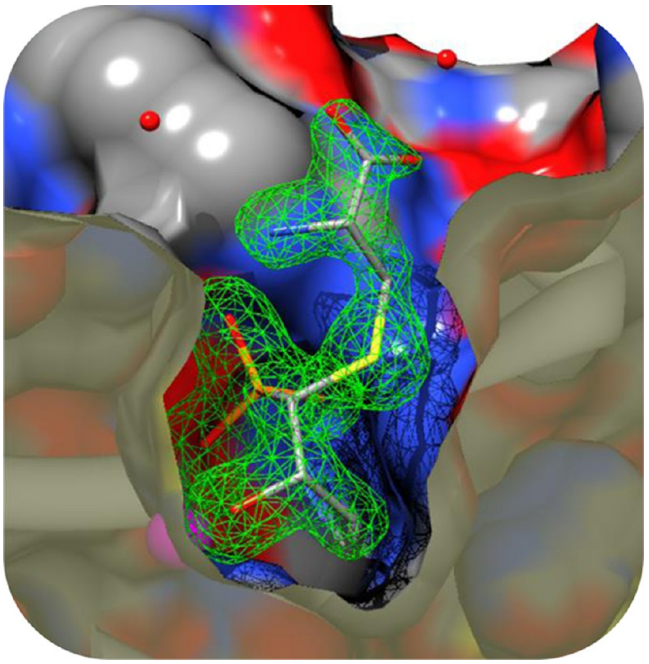

Figure 8. Active site of FosB^{Bc} in complex with Mn^{2+} and **2**, (1*R*,2*S*)-1-(*S*-L-cysteinyl)-2-hydroxypropylphosphonate, at 1.55 Å resolution (PDB 4JH7). In the final refinement, R_{work} = 13.33% and R_{free} = 18.64%. The difference electron density shown for **2** is the $2F_o-F_c$ map calculated before the addition of **2** to the coordinate file. It is contoured at 3σ and emphasizes the quality of the data. The C1 of fosfomycin is clearly sp^3 hybridized, and strong electron density is observed for the sulfur.

metal through one of the phosphonate oxygens and hydrogen bonded to Arg94, Arg124, Tyr64, and Tyr105 through the other two. The triangular cage structure around the phosphonate end is maintained by a salt bridge from Arg94 to Asp100 and hydrogen bonds from Arg124 to Tyr39 and Asp100. On the opposite end, the oxirane oxygen is coordinated to the metal such that the methyl group of fosfomycin is held adjacent to Trp46 and C2 of fosfomycin is pointed directly at Ala48. The amino acids that construct the fosmomycin cage structure and form hydrogen bonds to the antibiotic are conserved throughout all of the FosB enzymes (Figure S10, green).

The conserved residues, Arg94 and Asp100, that form the salt bridge of the loop region in FosB that encloses the phosphonate group of fosfomycin are not found in FosA (PA1129). Rather, in FosA (PA1129) the region (approximately aa 90−100) is composed of amino acids that form the potassium binding loop. K^+ is required for the optimum activation of FosA[11] but not for FosB.

Tyr39 is conserved in both the FosA and FosB enzymes. From the energy-minimized docking results, Tyr39 of FosA was reported to be in a favorable position to ionize GSH, being 3.45 Å away from the docked substrate thiol.[33] In both the FosB^{Bc}·Zn^{2+} ternary complex (PDB 4JH8) and the FosB^{Bc}·Mn^{2+}·**2** complex (PDB 4JH7), Tyr39 is located approximately 3.31 Å from the L-Cys sulfur, which is consistent with the docking results for GSH to FosA. Mutation of Tyr39 to phenylalanine in FosA (PA1129) resulted in a 13-fold reduction in enzymatic turnover and a 50-fold decrease in catalytic efficiency for the thiol substrate, k_{cat}/K_M^{GSH}.[33] Thus, the function of Tyr39, in either FosA or FosB, is likely to abstract a proton from and activate the incoming thiol during the reaction. Hydrogen bonding of Tyr39 to Arg124 (Figure 9) should stabilize the tyrosinate anion to facilitate this function.

Interestingly, the Cys9 residue of FosB^{Bc}, FosB^{Sa}, and FosB^{Ba} is not conserved in FosB^{Ss} (*Staphylococcus saprophyticus*) or FosB^{Bs} (Figure S10, red). FosB^{Ss} has a threonine at position 9,

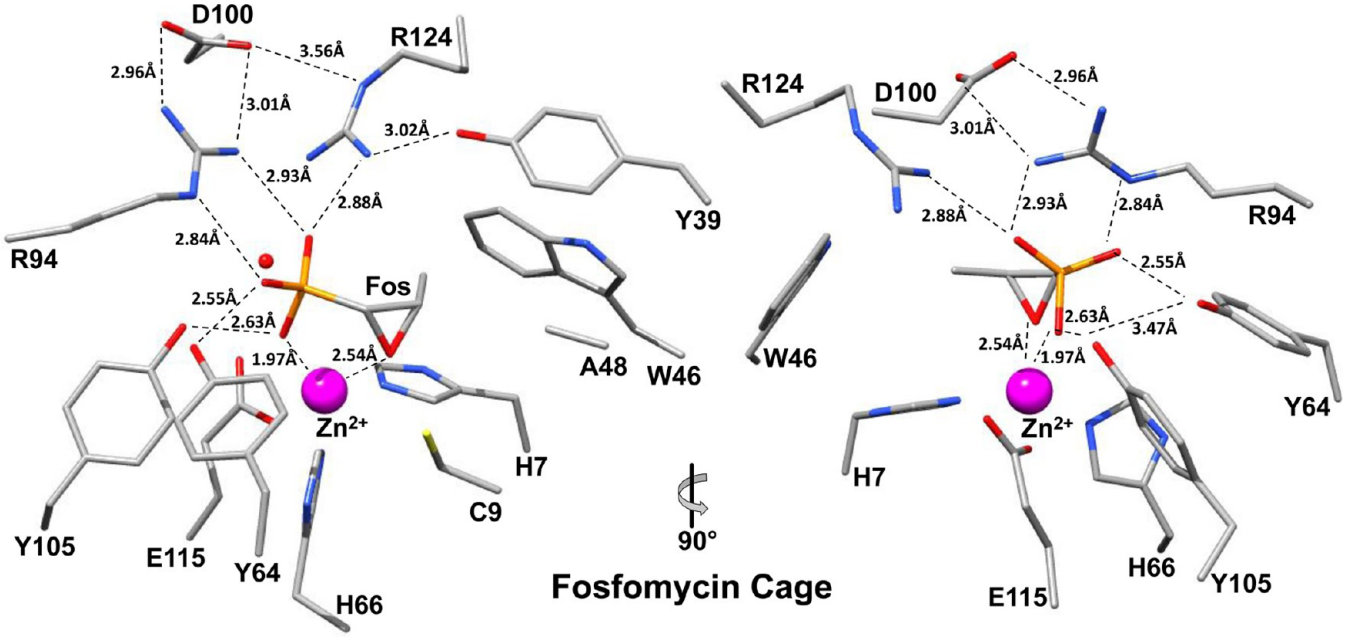

Figure 9. Fosfomycin molecule surrounded by a cage of amino acids. The cage has both a polar and nonpolar end to accommodate the antibiotic. The polar phosphonate group is coordinated to the metal through one of the phosphonate oxygens and is hydrogen bonded to Arg94, Arg124, Tyr64, and Tyr105 through the other two. On the opposite end, the oxirane oxygen is coordinated to the metal, and the hydrophobic methyl group of fosfomycin is held adjacent to Trp46. The amino acids that construct the fosmomycin cage are conserved throughout all of the FosB enzymes (Figure S10, green). This figure was made with PDB 4JH3.

dx.doi.org/10.1021/bi4009648 | *Biochemistry* 2013, 52, 7350−7362

the same as FosA (PA1129).[12] In FosA (PA1129), the Thr9 residue is proposed to activate the oxirane oxygen of fosfomycin. Similarly for FosB^{Bc}, FosB^{Sa}, and FosB^{Ba}, Cys9 has been proposed to active the oxirane oxygen. However, in FosB^{Bs}, there is no analogous amino acid at this position that could serve to activate the fosfomycin molecule. This lack in conservation at amino acid position 9 of the FosB enzymes suggests an alternative mode of activation of the epoxide oxygen of fosfomycin rather than simply protonation by either a hydroxyl or sulfhydryl side chain as previously suggested.[12]

Superposition of the FosB^{Bc}·Mn^{2+}·**1** (PDB 4JH6) and FosB^{Bc}·Mn^{2+}·**2** (PDB 4JH7) product structures provides some insight into the metal-ion assisted activation of the antibiotic. When the L-Cys thiol adds to C1 of fosfomycin and the epoxide ring opens, the Mn^{2+} metal displaces from the three coordinating amino acids such that the overall coordination geometry of Mn^{2+} changes (Figures 10 and S11 and Table 2). If

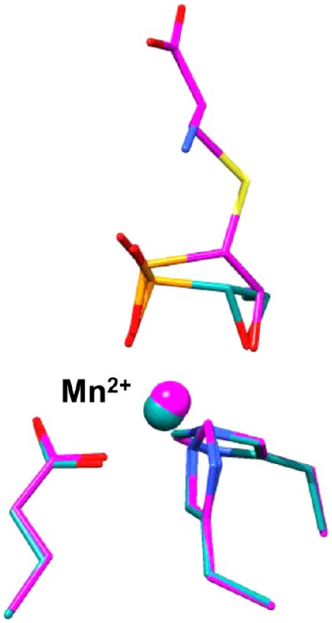

Figure 10. Superposition of the FosB^{Bc}·Mn^{2+}·**1** (PDB 4JH6) and FosB^{Bc}·Mn^{2+}·**2** (PDB 4JH7) structures. When the L-Cys thiol adds to C1 of fosfomycin and the epoxide ring opens, the Mn^{2+} metal displaces from the three coordinating amino acids such that the overall coordination geometry of Mn^{2+} changes. Specifically, the equatorial distances expand, and the metal−oxygen$_{(oxirane)}$ bond shortens, effectively creating a more symmetric trigonal bipyramidal geometry around Mn^{2+} and relieving strain on both the atomic orbitals of the metal and the epoxide ring of the antibiotic (Table 2).

Table 2. Metal−Ligand Distances for FosB^{Bc}·Mn^{2+}·1 and FosB^{Bc}·Mn^{2+}·2 (Å)

structure	Mn^{2+}−H7$_{N\varepsilon}$	Mn^{2+}−H66$_{N\varepsilon}$	Mn^{2+}−E115$_{O\varepsilon}$	Mn^{2+}−O$_{(phosphonate)}$	Mn^{2+}−O$_{(oxirane)}$
FosB^{Bc}·Mn^{2+}·**1**	2.08	2.03	2.04	1.91	2.51
FosB^{Bc}·Mn^{2+}·**2**	2.16	2.17	2.07	2.01	2.38

the *Z* axis is defined along E115O$_{\varepsilon}$−Mn^{2+}−Fosfomycin-O$_{(oxirane)}$ (Figures 11 and S11), then there is a distorted trigonal bipyramidal geometry about the Mn^{2+} center similar to that observed in FosA. When the product is formed, the equatorial distances expand, and the metal−oxygen$_{(oxirane)}$ bond

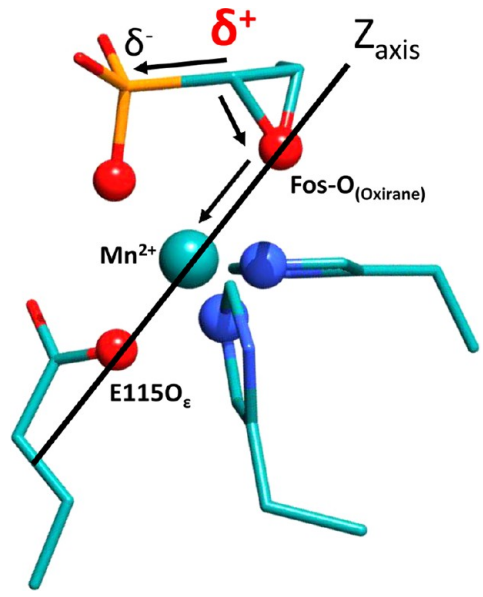

Figure 11. Activation of fosfomycin occurs through σ donation of the epoxide lone pair into the d_z^2 orbital of Mn^{2+}, significantly increasing the polarity of the C1−O$_{(oxirane)}$ bond and resulting in greater partial positive charge (δ^+) on C1. In addition, the electron-withdrawing nature of the phosphonate group will further enhance δ^+ on C1 through polarization of the C1−P bond. Arrows denote electron charge redistribution away from C1 to both the phosphonate and the epoxide oxygen. This primes the antibiotic for nucleophilic attack by the thiol substrate. This figure was made with PDB 4JH6.

shortens, effectively creating a more symmetric trigonal bipyramidal geometry around Mn^{2+} and relieving strain on both the atomic orbitals of the metal and the epoxide ring of the antibiotic. The observed changes in metal−ligand bond distances are on the order of approximately 0.1 Å. These observable deviations are justified given that the estimated overall coordinate errors from maximum likelihood refinement are 0.03 and 0.04 Å for the FosB^{Bc}·Mn^{2+}·**1** and FosB^{Bc}·Mn^{2+}·**2** structures, respectively. Furthermore, the estimated upper limits of atomic coordinate errors are 0.04 and 0.05 Å for the FosB^{Bc}·Mn^{2+}·**1** and FosB^{Bc}·Mn^{2+}·**2** structures, respectively, as calculated from Luzzati plots in the PDB validation reports.

Although the original investigation of FosB^{Bs} with L-Cys as the thiol has a slightly different activation order, Zn^{2+} was effectively shown to be an inhibitor of L-Cys transferase activity. Such similarity of metal activation by Mn^{2+} across the fosfomycin resistance enzyme classes warrants further explanation. Preferential activation of the fosfomycin resistance proteins (including FosA, FosB, and FosX) by Mn^{2+} over the other divalent transition metals tested can be explained by the hard and soft acid and base (HSAB) theory.[34] In this context, Mn^{2+} is a hard acid, and the lone pair electrons on the oxirane oxygen of fosfomycin are a hard base; Ni^{2+} and Zn^{2+} are both defined as borderline, with Zn^{2+} being the softest.[34] Thus, Mn^{2+} will form the strongest Lewis acid/base complex with the oxirane oxygen lone pair. Defining the *Z* axis of the metal along E115O$_{\varepsilon}$−Mn^{2+}−Fosfomycin-O$_{(oxirane)}$ (Figures 11 and S11) positions the d_z^2 orbital of Mn^{2+} to be the lone pair acceptor orbit. Furthermore, the lone pair on the oxirane oxygen is an excellent σ donor for the d_z^2 orbital of Mn^{2+}, resulting in a very strong σ-type interaction between the ligand and the metal.

Strong σ donation of the epoxide lone pair into the d_z^2 orbital of Mn^{2+} will significantly increase the polarity of the

dx.doi.org/10.1021/bi4009648 | Biochemistry 2013, 52, 7350−7362

C1−$O_{(oxirane)}$ bond of fosfomycin, resulting in greater partial positive charge (δ^+) on C1. In addition, the electron-withdrawing nature of the phosphonate group will further enhance δ^+ on C1 through polarization of the C1−P bond. Electron charge redistribution away from C1 to both the phosphonate and the epoxide oxygen significantly increases the δ^+ on C1 and primes the antibiotic for nucleophilic attack by the thiolate substrate (Figure 11).

In the Mn^{2+}·$FosB^{Bc}$·**2** structure, O_δ of Asn50 is 3.80 Å from C1 of **2** and N_δ of Asn50 3.61 Å from the thioether of **2** averaged over the two active sites. These distances are on the edge of van der Waals interactions for the nuclei. Asn50 is also conserved throughout the FosB enzymes (Figure S10, red) but not in FosA. In FosA (PA1129), the position is occupied by a serine residue (Ser50) that has been implicated in GSH binding.[33] However, in the FosB enzymes, the asparagine at position 50 likely serves to stabilize the incoming L-Cys^- or BS^- negative charge as well as the δ^+ on C1 of fosfomycin during nucleophilic attack. Comparison of the of the Zn^{2+}·$FosB^{Bc}$·**1**·L-Cys ternary complex and Mn^{2+}·$FosB^{Bc}$·**2** product structures clearly shows that Asn50 adopts two conformations, one perpendicular (ternary complex) and one nearly parallel (product complex) to the C1−S bond of the L-Cys-fosfomycin product (Figure 6), the same orientation as it is observed in the other seven structures whether fosfomycin is present or not. The latter orientation is maintained by a hydrogen bond between O_δ of Asn50 and the thiol of the adjacent Cys9 in the active site. Rotation of Asn50 about the C_β−C_γ bond is the only significant variation observed in the reported structures of $FosB^{Bc}$. The unique conformation is locked by hydrogen bonds between O_δ of Asn50 and the primary amine of the exogenous L-Cys and between N_δ of Asn50 and the backbone carbonyl of Leu49. This orientation positions O_δ of Asn50 4.13 Å from C1 of fosfomycin and N_δ of Asn50 4.20 Å from the L-Cys thiol, well beyond van der Waals range. Thus, in $FosB^{Bc}$, Tyr39 and Asn50 work in a concerted manner to ionize and stabilize the approaching thiolate during the reaction (Figure 6).

The same rationale for why this family of fosfomycin resistance enzymes is activated by Mn^{2+} can be used to explain why the enzymes, including FosA and FosX, are the least activated or even inhibited by Zn^{2+}. Zn^{2+} is the softest acid of the metals tested and will therefore form the weakest Lewis acid/base complex with the lone pair electrons of the oxirane oxygen. Furthermore, given that Zn^{2+} is a d^{10} metal species, the d_{z^2} orbital is full and therefore unable to accept electron donation from the lone pair, resulting in a decreased δ^+ on C1 of fosfomycin. Therefore, even though Zn^{2+} is the strongest Lewis acid of the metals tested, it will form the weakest Lewis acid/base complex with the oxirane lone pair of fosfomycin because of the energetically unfavorable soft−hard combination.

CONCLUSIONS

The mechanism of $FosB^{Bc}$ is acid-catalyzed nucleophilic epoxide ring-opening, where Mn^{2+} serves as the Lewis acid. Fosfomycin is activated by the formation of a strong Lewis acid/base complex with Mn^{2+}. The resultant complex serves to enhance δ^+ on C1 through polarization of the C1−$O_{(oxirane)}$ bond in addition to the already polarized C1−P bond of the antibiotic. Tyr39 facilitates ionization of the incoming thiol, while Asn50 stabilizes both the δ^+ on C1 of fosfomycin and S^- of the incoming nucleophile. Inversion of configuration at C1 indicates that the reaction proceeds via direct S_N2 addition of the thiol to the oxirane carbon, forming the same (1*R*,2*S*)-1-(*S*-L-cysteinyl)-2-hydroxypropylphosphonate (or (1*R*,2*S*)-1-(*S*-bacillithiolyl)-2-hydroxypropylphosphonate) product as that formed by FosA.[31]

Antibiotic modifying enzymes represent a common mode of microbial resistance and are, therefore, obvious targets for the development of new therapeutic agents. Characterizing the interaction between resistance enzymes and their cosubstrates is a critical step toward the discovery of lead compounds to combat antimicrobial resistant bacteria. The L-Cys-fosfomycin product structure confirms the role of the solvent channel in $FosB^{Bc}$ and represents a major contribution in understanding the mechanism of the enzyme. However, given that BSH is the preferred substrate of FosB over L-Cys, part of the thermodynamic driving force of the reaction must be the interaction of the enzyme with the glucosamine-malate portion of BSH. To target FosB therapeutically, this interaction must still be characterized.

ASSOCIATED CONTENT

Supporting Information

Active site residues that define the metal-ion and sulfate binding sites from the X-ray crystal structure of the FosB protein from *Bacillus cereus* in complex with Zn^{2+} and sulfate at 1.55 Å resolution. Active site residues that define the metal-ion and fosfomycin binding sites from the second crystal structure of $FosB^{Bc}$ in complex with Zn^{2+} and fosfomycin at 1.49 Å resolution. Overall X-ray crystal structure of $FosB^{Bc}$ in complex with Zn^{2+} and fosfomycin at 1.50 Å resolution. Overall X-ray crystal structure of $FosB^{Bc}$ in complex with Ni^{2+} and fosfomycin at 1.89 Å resolution. Overall X-ray crystal structure of $FosB^{Bc}$ in complex with Co^{2+} and fosfomycin at 1.77 Å resolution. X-ray fluorescence scans of the $FosB^{Bc}$·Zn^{2+}, $FosB^{Bc}$·Ni^{2+}−fosfomycin, $FosB^{Bc}$·Co^{2+}−fosfomycin, and $FosB^{Bc}$·Mn^{2+}−fosfomycin crystals. Active site of $FosB^{Bc}$ in complex with Mn^{2+} in the presence of **3** at 1.77 Å resolution. Sequence alignment of current FosB enzymes. Comparison of the $FosB^{Bc}$·Mn^{2+}·**1** and $FosB^{Bc}$·Mn^{2+}·**2** structures. This material is available free of charge via the Internet at http://pubs.acs.org.

Accession Codes

The atomic coordinates and structure factors for structures reported in this work have been deposited in the Protein Data Bank under file names 4JH1, 4JH2, 4JH3, 4JH4, 4JH5, 4JH6, 4JH7, 4JH8, and 4JH9.

AUTHOR INFORMATION

Corresponding Author

*Email: r.armstrong@vanderbilt.edu. Phone: (615) 343-2920.

Funding

This work was supported by grants R01 GM030910 to R.N.A., T32 ES007028 to M.K.T. and M.E.K., and F32 GM093507 to P.D.C. from the National Institutes of Health. The use of the Advanced Photon Source, an Office of Science User Facility operated for the U.S. Department of Energy (DOE) Office of Science by Argonne National Laboratory, was supported by the U.S. DOE under contract no. DE-AC02-06CH11357. The use of the LS-CAT Sector 21 was supported by the Michigan Economic Development Corporation and the Michigan Technology Tri-Corridor (grant 085P1000817).

Notes

The authors declare no competing financial interest.

■ ACKNOWLEDGMENTS

M.K.T. thanks the William N. Pearson Fellowship in Biochemistry provided by Vanderbilt University.

■ REFERENCES

(1) Hendlin, D., et al. (1969) Phosphonomycin, a new antibiotic produced by strains of streptomyces. *Science 166*, 122−123.
(2) Eschenburg, S., Kabsch, W., Healy, M. L., and Schoenbrunn, E. (2003) A new view of the mechanisms of UDP-N-acetylglucosamine enolpyruvyl transferase (MurA) and 5-enolpyruvylshikimate-3-phosphate synthase (AroA) derived from X-ray structures of their tetrahedral reaction intermediate states. *J. Biol. Chem. 278*, 49215−49222.
(3) Eschenburg, S., Priestman, M., and Schoenbrunn, E. (2005) Evidence that the fosfomycin target Cys115 in UDP-N-acetylglucosamine enolpyruvyl transferase (MurA) is essential for product release. *J. Biol. Chem. 280*, 3757−3763.
(4) Eschenburg, S., Priestman, M. A., Abdul-Latif, F. A., Delachaume, C., Fassy, F., and Schoenbrunn, E. (2005) A novel inhibitor that suspends the induced fit mechanism of UDP-N-acetylglucosamine enolpyruvyl transferase (MurA). *J. Biol. Chem. 280*, 14070−14075.
(5) Falagas, M. E., Giannopoulou, K. P., Kokolakis, G. N., and Rafailidis, P. I. (2008) Fosfomycin: Use beyond urinary tract and gastrointestinal infections. *Clin. Infect. Dis. 46*, 1069−1077.
(6) Falagas, M. E., Kastoris, A. C., Karageorgopoulos, D. E., and Rafailidis, P. I. (2009) Fosfomycin for the treatment of infections caused by multidrug-resistant non-fermenting Gram-negative bacilli: A systematic review of microbiological, animal and clinical studies. *Int. J. Antimicrob. Agents 34*, 111−120.
(7) Patel, S. S., Balfour, J. A., and Bryson, H. M. (1997) Fosfomycin tromethamine. A review of its antibacterial activity, pharmacokinetic properties and therapeutic efficacy as a single-dose oral treatment for acute uncomplicated lower urinary tract infections. *Drugs 53*, 637−656.
(8) Arca, P., Hardisson, C., and Suarez, J. E. (1990) Purification of a glutathione S-transferase that mediates fosfomycin resistance in bacteria. *Antimicrob. Agents Chemother. 34*, 844−848.
(9) Arca, P., Rico, M., Brana, A. F., Villar, C. J., Hardisson, C., and Suarez, J. E. (1988) Formation of an adduct between fosfomycin and glutathione: A new mechanism of antibiotic resistance in bacteria. *Antimicrob. Agents Chemother. 32*, 1552−1556.
(10) Bernat, B. A., Laughlin, L. T., and Armstrong, R. N. (1997) Fosfomycin resistance protein (FosA) is a manganese metalloglutathione transferase related to Glyoxalase I and the extradiol dioxygenases. *Biochemistry 36*, 3050−3055.
(11) Bernat, B. A., Laughlin, L. T., and Armstrong, R. N. (1999) Elucidation of a monovalent cation dependence and characterization of the divalent cation binding site of the fosfomycin resistance protein (FosA). *Biochemistry 38*, 7462−7469.
(12) Rife, C. L., Pharris, R. E., Newcomer, M. E., and Armstrong, R. N. (2002) Crystal structure of a genomically encoded fosfomycin resistance protein (FosA) at 1.19 Å resolution by MAD phasing off the L-III Edge of Tl+. *J. Am. Chem. Soc. 124*, 11001−11003.
(13) Fillgrove, K. L., Pakhomova, S., Schaab, M. R., Newcomer, M. E., and Armstrong, R. N. (2007) Structure and mechanism of the genomically encoded fosfomycin resistance protein, FosX, from Listeria monocytogenes. *Biochemistry 46*, 8110−8120.
(14) Fillgrove, K. L., Pakhomova, S., Newcomer, M. E., and Armstrong, R. N. (2003) Mechanistic diversity of fosfomycin resistance in pathogenic microorganisms. *J. Am. Chem. Soc. 125*, 15730−15731.
(15) Cao, M., Bernat, B. A., Wang, Z., Armstrong, R. N., and Helmann, J. D. (2001) FosB, a cysteine-dependent fosfomycin resistance protein under the control of σW, an extracytoplasmic-function σ factor in Bacillus subtilis. *J. Bacteriol. 183*, 2380−2383.
(16) Rigsby, R. E., Fillgrove, K. L., Beihoffer, L. A., and Armstrong, R. N. (2005) Fosfomycin resistance proteins: A nexus of glutathione transferases and epoxide hydrolases in a metalloenzyme superfamily. *Methods Enzymol. 401*, 367−379.
(17) Lamers, A. P., Keithly, M. E., Kim, K., Cook, P. D., Stec, D. F., Hines, K. M., Sulikowski, G. A., and Armstrong, R. N. (2012) Synthesis of bacillithiol and the catalytic selectivity of FosB-type fosfomycin resistance proteins. *Org. Lett. 14*, 5207−5209.
(18) Newton, G. L., Rawat, M., La, C. J. J., Jothivasan, V. K., Budiarto, T., Hamilton, C. J., Claiborne, A., Helmann, J. D., and Fahey, R. C. (2009) Bacillithiol is an antioxidant thiol produced in bacilli. *Nat. Chem. Biol. 5*, 625−627.
(19) Newton, G. L., Fahey, R. C., and Rawat, M. (2012) Detoxification of toxins by bacillithiol in Staphylococcus aureus. *Microbiology 158*, 1117−1126.
(20) Gaballa, A., Newton, G. L., Antelmann, H., Parsonage, D., Upton, H., Rawat, M., Claiborne, A., Fahey, R. C., and Helmann, J. D. (2010) Biosynthesis and functions of bacillithiol, a major low-molecular-weight thiol in bacilli. *Proc. Natl. Acad. Sci. U.S.A. 107*, 6482−6486.
(21) Otwinowski, Z., and Minor, W. (1997) Processing of X-ray diffraction data collected in oscillation mode. *Methods Enzymol. 276*, 307−326.
(22) McCoy, A. J., Grosse-Kunstleve, R. W., Adams, P. D., Winn, M. D., Storoni, L. C., and Read, R. J. (2007) Phaser crystallographic software. *J. Appl. Crystallogr. 40*, 658−674.
(23) Sheldrick, G. M. (2008) A short history of SHELX. *Acta Crystallogr., Sect. A 64*, 112−122.
(24) Langer, G., Cohen, S. X., Lamzin, V. S., and Perrakis, A. (2008) Automated macromolecular model building for X-ray crystallography using ARP/wARP version 7. *Nat. Protoc. 3*, 1171−1179.
(25) Emsley, P., and Cowtan, K. (2004) Coot: Model-building tools for molecular graphics. *Acta Crystallogr., Sect. D D60*, 2126−2132.
(26) Murshudov, G. N., Vagin, A. A., and Dodson, E. J. (1997) Refinement of macromolecular structures by the maximum-likelihood method. *Acta Crystallogr., Sect. D D53*, 240−255.
(27) Pettersen, E. F., Goddard, T. D., Huang, C. C., Couch, G. S., Greenblatt, D. M., Meng, E. C., and Ferrin, T. E. (2004) UCSF Chimera-A visualization system for exploratory research and analysis. *J. Comput. Chem. 25*, 1605−1612.
(28) Schuttelkopf, A. W., and van, A. D. M. F. (2004) PRODRG: A tool for high-throughput crystallography of protein-ligand complexes. *Acta Crystallogr., Sect. D 60*, 1355−1363.
(29) Pakhomova, S., Rife, C. L., Armstrong, R. N., and Newcomer, M. E. (2004) Structure of fosfomycin resistance protein FosA from transposon Tn2921. *Protein Sci. 13*, 1260−1265.
(30) Armstrong, R. N. (2000) Mechanistic diversity in a metalloenzyme superfamily. *Biochemistry 39*, 13625−13632.
(31) Bernat, B. A., Laughlin, L. T., and Armstrong, R. N. (1998) Regiochemical and stereochemical course of the reaction catalyzed by the fosfomycin resistance protein, FosA. *J. Org. Chem. 63*, 3778−3780.
(32) Roberts, A. A., Sharma, S. V., Strankman, A. W., Duran, S. R., Rawat, M., and Hamilton, C. J. (2013) Mechanistic studies of FosB: A divalent-metal-dependent bacillithiol-S-transferase that mediates fosfomycin resistance in Staphylococcus aureus. *Biochem. J. 451*, 69−79.
(33) Rigsby, R. E., Brown, D. W., Dawson, E., Lybrand, T. P., and Armstrong, R. N. (2007) A model for glutathione binding and activation in the fosfomycin resistance protein, FosA. *Arch. Biochem. Biophys. 464*, 277−283.
(34) Pearson, R. G. (1968) Hard and soft acids and bases (HSAB). I. Fundamental principles. *J. Chem. Educ. 45*, 581−587.